REFERENCES AND NOTES

1. S. P. Grand, *Philos. Trans. A Math. Phys. Eng. Sci.* **360**, 2475–2491 (2002).
2. N. A. Simmons, A. M. Forte, S. P. Grand, *Geophys. J. Int.* **177**, 1284–1304 (2009).
3. L. Liu, S. Spasojević, M. Gurnis, *Science* **322**, 934–938 (2008).
4. T. W. Becker, C. Faccenna, E. D. Humphreys, A. R. Lowry, M. S. Miller, *Earth Planet. Sci. Lett.* **402**, 234–246 (2014).
5. M. Roy, T. H. Jordan, J. Pederson, *Nature* **459**, 978–982 (2009).
6. J. W. van Wijk *et al.*, *Geology* **38**, 611–614 (2010).
7. L. Liu, M. Gurnis, *Geology* **38**, 663–666 (2010).
8. A. Levander *et al.*, *Nature* **472**, 461–465 (2011).
9. L. M. Flesch, W. E. Holt, A. J. Haines, B. Shen-Tu, *Science* **287**, 834–836 (2000).
10. A. Ghosh, W. E. Holt, *Science* **335**, 838–843 (2012).
11. N. Flament, M. Gurnis, R. D. Müller, *Lithosphere* **5**, 189–210 (2013).
12. L. Liu, *Rev. Geophys.* **53**, 1022–1049 (2015).
13. D. Hasterok, D. S. Chapman, *Earth Planet. Sci. Lett.* **307**, 59–70 (2011).
14. Incorporated Research Institutions in Seismology Data Management Center, Data Services Products: EARS EarthScope Automated Receiver Survey (IRIS, 2010); http://ds.iris.edu/ds/products/ears/.
15. R. E. M. Riva, R. Govers, *Geophys. J. Int.* **176**, 614–624 (2009).
16. M. I. Billen, *Annu. Rev. Earth Planet. Sci.* **36**, 325–356 (2008).
17. D. L. Kohlstedt, B. K. Holtzman, *Annu. Rev. Earth Planet. Sci.* **37**, 561–593 (2009).
18. A. Pommier *et al.*, *Geochem. Geophys. Geosyst.* **14**, 1685–1692 (2013).
19. S. Mei, W. Bai, T. Hiraga, D. L. Kohlstedt, *Earth Planet. Sci. Lett.* **201**, 491–507 (2002).
20. S. Chen, T. Hiraga, D. L. Kohlstedt, *J. Geophys. Res.* **111** (B8), B08203 (2006).
21. L. Xu *et al.*, *Earth Planet. Sci. Lett.* **379**, 158–165 (2013).
22. E. Gardés, F. Gaillard, P. Tarits, *Geochem. Geophys. Geosyst.* **15**, 4984–5000 (2014).
23. S. Karato, H. Jung, *Philos. Mag.* **83**, 401–414 (2003).
24. D. Wang, M. Mookherjee, Y. Xu, S. Karato, *Nature* **443**, 977–980 (2006).
25. P. E. Wannamaker *et al.*, *Geochem. Geophys. Geosyst.* **9**, Q05019 (2008).
26. Methods and data processing techniques are available in the supplementary materials on *Science* Online.
27. D. Hasterok, D. S. Chapman, *J. Geophys. Res.* **112**, B06415 (2007).
28. W. C. Hammond, W. Thatcher, *J. Geophys. Res.* **109** (B8), B08403 (2004).
29. A. R. Lowry, R. B. Smith, *J. Geophys. Res.* **99** (B10), 20123–20140 (1994).
30. N. M. Meqbel, G. D. Egbert, P. E. Wannamaker, A. Kelbert, A. Schultz, *Earth Planet. Sci. Lett.* **402**, 290–304 (2014).

ACKNOWLEDGMENTS

The authors thank J. Hu for helping with the non-Newtonian rheology. L.L. is supported by NSF grants EAR-1554554 and ACI-1516586. Collection of MT data and support for D.H. are provided by NSF grants to P. E. Wannamaker EAR81-16602, 84-17765, and 02-30027. L.L. conceived the project and performed the geodynamic calculations. D.H. provided expertise on MT-sounding and lithosphere buoyancy. Both authors contributed to manuscript preparation. MT data are available in reference (*25*). Additional information on the geodynamic modeling is available in the supplementary materials.

SUPPLEMENTARY MATERIALS

www.sciencemag.org/content/353/6307/1515/suppl/DC1
Materials and Methods
Supplementary Text
Figs. S1 to S7
References (*31*–*34*)

9 March 2016; accepted 24 August 2016
10.1126/science.aaf6542

PROTOPLANETARY DISKS

Spiral density waves in a young protoplanetary disk

Laura M. Pérez,[1]* John M. Carpenter,[2] Sean M. Andrews,[3] Luca Ricci,[3] Andrea Isella,[4] Hendrik Linz,[5] Anneila I. Sargent,[6] David J. Wilner,[3] Thomas Henning,[5] Adam T. Deller,[7] Claire J. Chandler,[8] Cornelis P. Dullemond,[9] Joseph Lazio,[10] Karl M. Menten,[1] Stuartt A. Corder,[2] Shaye Storm,[3] Leonardo Testi,[11,12] Marco Tazzari,[11] Woojin Kwon,[13,14] Nuria Calvet,[15] Jane S. Greaves,[16] Robert J. Harris,[17] Lee G. Mundy[18]

Gravitational forces are expected to excite spiral density waves in protoplanetary disks, disks of gas and dust orbiting young stars. However, previous observations that showed spiral structure were not able to probe disk midplanes, where most of the mass is concentrated and where planet formation takes place. Using the Atacama Large Millimeter/submillimeter Array, we detected a pair of trailing symmetric spiral arms in the protoplanetary disk surrounding the young star Elias 2-27. The arms extend to the disk outer regions and can be traced down to the midplane. These millimeter-wave observations also reveal an emission gap closer to the star than the spiral arms. We argue that the observed spirals trace shocks of spiral density waves in the midplane of this young disk.

Spiral density waves are expected to be excited in the midplane of protoplanetary disks by the action of gravitational forces, generated by, for example, planet-disk interactions (*1*) or gravitational instabilities (*2*). These waves give rise to a spiral structure whose observable characteristics—the number and location of arms and their amplitudes and pitch angles—depend on the driving mechanism and the disk physical properties (*1*, *3*–*5*). Theoretical predictions agree that these spiral features can be very prominent and thus more easily observable than the putative embedded planets or instabilities driving such waves (*6*, *7*). Spiral-like patterns have been observed in evolved protoplanetary disks with depleted inner regions, in optical scattered light (*8*–*13*) or gas spectral lines (*14*, *15*). However, at the wavelength of such observations the emission is optically thick, and scattered light only traces the tenuous surface layers of these disks rather than their midplane densities. This makes it impossible to disentangle between minute perturbations near the disk surface and true density enhancements over the disk column attributable to spiral density waves (*5*, *16*). To probe the disk density structure, particularly the disk midplane that contains most of the mass and where planets form, observations of optically thin emission are necessary.

We used the Atacama Large Millimeter/submillimeter Array (ALMA) to observe the protoplanetary disk around the young star Elias 2-27 at a wavelength of 1.3 mm. Our spatially resolved image (Fig. 1) shows two symmetric spiral arms extending from an elliptical emission ring. To emphasize the spirals and the dark ring of attenuated emission seen at ≈70-astronomical-unit (AU) radial distance from the star, we applied an unsharp masking filter (*17*) to increase substantially the image contrast (Fig. 1B).

The young star Elias 2-27 (*18*) is a member of the ρ-Ophiuchus star-forming complex at a distance of 139 pc (*19*) and is classified as a class II young stellar object from analysis of its spectral energy distribution (SED) (*20*, *21*). Although the star is only 50 to 60% of the Sun's mass ($M_{\odot}$) (*20*, *22*), it is known to harbor an unusually massive [0.04 to 0.14 $M_{\odot}$ (*20*, *23*, *24*)] protoplanetary disk. The star, obscured by 15 magnitudes of extinction at optical wavelengths by the

[1]Max-Planck-Institut für Radioastronomie, Auf dem Hügel 69, 53121 Bonn, Germany. [2]Joint Atacama Large Millimeter/submillimeter Array (ALMA) Observatory, Avenida Alonso de Córdova 3107, Vitacura, Santiago, Chile. [3]Harvard-Smithsonian Center for Astrophysics, 60 Garden Street, Cambridge, MA 02138, USA. [4]Rice University, 6100 Main Street, Houston, TX 77005, USA. [5]Max-Planck-Institut für Astronomie, Königstuhl 17, 69117 Heidelberg, Germany. [6]California Institute of Technology, 1200 East California Boulevard, Pasadena, CA 91125, USA. [7]Netherlands Institute for Radio Astronomy (ASTRON), 7990-AA Dwingeloo, Netherlands. [8]National Radio Astronomy Observatory, Post Office Box O, Socorro, NM 87801, USA. [9]Heidelberg University, Center for Astronomy, Albert Ueberle Strasse 2, Heidelberg, Germany. [10]Jet Propulsion Laboratory, California Institute of Technology, 4800 Oak Grove Drive, Pasadena, CA 91106, USA. [11]European Southern Observatory, Karl Schwarzschild Strasse. 2, 85748 Garching, Germany. [12]Istituto Nazionale di Astrofisica (INAF)–Osservatorio Astrofisico di Arcetri, Largo E. Fermi 5, 50125 Firenze, Italy. [13]Korea Astronomy and Space Science Institute, 776 Daedeokdae-ro, Yuseong-gu, Daejeon 34055, Republic of Korea. [14]Korea University of Science and Technology, 217 Gajeong-ro, Yuseong-gu, Daejeon 34113, Republic of Korea. [15]University of Michigan, 830 Dennison Building, 500 Church Street, Ann Arbor, MI 48109, USA. [16]Cardiff University, School of Physics and Astronomy, 4 The Parade, Cardiff CF24 3AA, UK. [17]University of Illinois, 1002 West Green Street, Urbana, IL 61801, USA. [18]Department of Astronomy, University of Maryland, College Park, MD 20742, USA.
*Corresponding author. Email: lperez@mpifr-bonn.mpg.de

parent molecular cloud (*22*), accretes material from its surrounding disk with a mass accretion rate of 8×10^{-8} $M_\odot$ year^{-1} (*25*). Previous observations at 0.6″ to 1.1″ angular resolution were well described by a smooth and axisymmetric distribution of material in the disk that extends near the stellar photosphere and decreases monotonically with distance from the star (*20*, *23*).

To estimate the optical depth of the observed dust continuum emission, we performed radiative transfer calculations using RADMC-3D (*26*) at 1.3 mm (*17*), using the previous surface density constraint found for the Elias 2-27 disk (*20*). This model reproduces the azimuthally averaged radial profile of the observed ALMA 1.3-mm continuum emission (fig. S1) (*17*). At a radial distance from the star (hereafter referred to as radius and denoted by R) larger than $R \approx 10$ AU, the emission is optically thin and thus traces the density of solid material down to the midplane of the disk. At the location of the spiral structures (from R = 100 to 300 AU), the azimuthally averaged optical depth τ of the dust continuum emission is $\tau = 0.1$ at R = 100 AU, decreasing to $\tau = 0.02$ at R = 300 AU (fig. S1B), which is consistent with the measured peak brightness temperature on the spirals of 1.2 K at R = 150 AU.

The spiral structures are even more evident in Fig. 2A, in which the data has been projected into a polar coordinate grid that accounts for the viewing geometry of the disk. In polar coordinates, a ring with zero eccentricity would have a constant radius for all polar angles. However, shown in Fig. 2A are two bright structures that grow in radius from ~100 to 300 AU as the polar angle increases. The brightest of these two structures lies northwest of the star, labeled "NW"; the spiral structure southeast of the star is labeled "SE." In Fig. 2B, we present the surface brightness contrast of the NW and SE arms, defined as the ratio between the peak of emission at the arm and the background surface brightness (*17*). We found that both arms have similar contrasts ranging between values of 1.3 and 2.5. The spiral arms reach their highest contrast at R = 150 AU, coinciding with the location in the disk where gravity has the most influence over thermal pressure and shear forces, that is, where the Toomre Q parameter is lowest (fig. S2) (*17*). However, even at its minimum value Toomre Q is well inside the stable regime (*17*). If the spirals arms suffer from beam dilution (if their physical size is smaller than the angular resolution of our observation), a higher optical depth than our previous estimate could be possible, implying an even higher density contrast in the arms. Thus, the contrast values measured for NW and SE are lower limits.

We determined the local maxima and minima of emission in the dust continuum observations at evenly spaced azimuthal angles, after subtracting a smooth monotonically decreasing intensity profile that best fit the intensity radial profile of the disk (fig. S3) (*17*). As demonstrated in Fig. 3, the emission local maxima (Fig. 3, crosses) describe two spiral structures, whereas the emission local minima (Fig. 3, circles) describe an ellipse. We

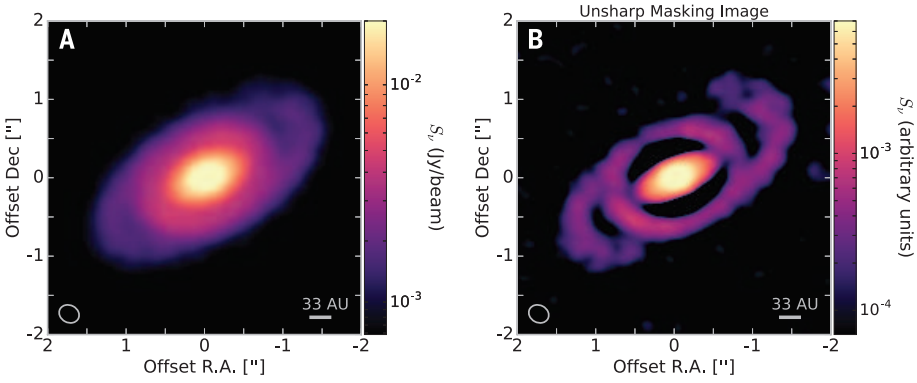

Fig. 1. Thermal dust emission from the protoplanetary disk surrounding Elias 2-27. The disk was imaged at a wavelength of 1.3 mm, with ALMA reaching an angular resolution of 0.26″ by 0.22″ (indicated by the ellipse in the bottom left corner), which corresponds to 36 by 31 AU at the distance of the star. The field-of-view center (at 0, 0) corresponds to the disk emission peak located at right ascension (J2000) = 16 hours 26 min 45.024 s, declination (J2000) = −24 degrees 23 min 08.250 s, and coincidental with the position of the star Elias 2-27. (**A**) 1.3-mm dust continuum image from the Elias 2-27 protoplanetary disk over a 4″ by 4″ area. The color scale represents flux density measured in units of Jansky per beam (1 Jy = 10^{-26} W m^{-2} Hz^{-1}). (**B**) Increased contrast image from processing the original ALMA observations shown in (A) with an unsharp masking filter (*17*).

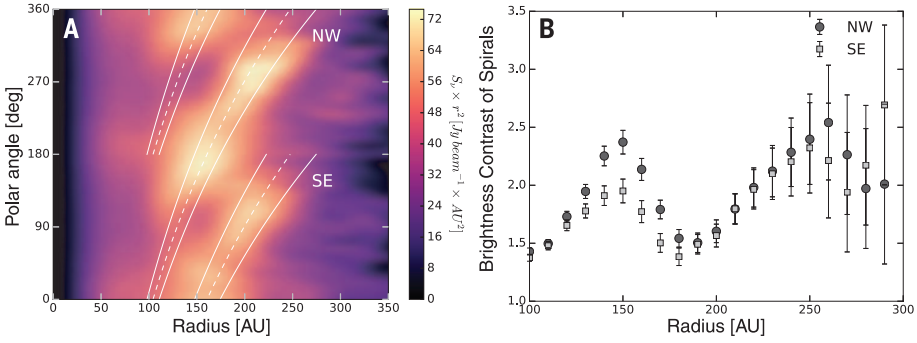

Fig. 2. Polar projection of disk emission and measured contrast over the spirals in the Elias 2-27 protoplanetary disk. (**A**) Projection onto polar coordinates (polar angle θ versus deprojected radial distance to the central star R) of the dust continuum observations from the Elias 2-27 disk. The emission has been scaled by R^2 in order to aid visualization, and the polar angle is defined as θ = 0° (north) increasing toward east. Curves correspond to the best-fit model spirals for the NW and SE arms (dashed lines) and their constraint at the 3σ level (solid lines). (**B**) Surface brightness contrast of the continuum emission along each spiral arm, defined as the ratio between the peak of emission and the background surface brightness (*17*), which is computed at increasing radial distance from the star.

constrained the geometry of these structures by modeling their location in polar coordinates (where R is the distance from the star located at the origin and θ is the angle from the x axis), taking into account that these structures have been inclined and rotated with respect to our line of sight by their inclination (i) and position angle (PA). The emission local minima were fitted with a circular ring ($R = a_0$, where a_0 is the radius at which the gap is located), whereas the emission local maxima were fitted with two symmetric logarithmic spirals ($R = R_0\, e^{b\theta}$, where R_0 is the spiral radius at θ = 0°, and b is the rate at which the spirals increase their distance from the origin). The best-fit parameters for the symmetric spirals that describe the local maxima are $R_0 = 84 \pm 4$ AU and $b = 0.138 \pm 0.007$ (which corresponds to a pitch angle of $\phi = 7.9° \pm 0.4°$), whereas the circular ring that describes the local minima has a radius of $a_0 = 71 \pm 2$ AU. The geometry of the spiral arms and dark ring can all be described with a single inclination angle of $i = 55.8° \pm 0.9°$ and position angle $PA = 117.3° \pm 0.9°$. The best-fit model and constraints at the 3σ level are shown in Fig. 3 for the spiral arms and dark ring.

Spatially resolved molecular line observations of CO and two isotopologues, simultaneous to the continuum observations discussed here, suggest that the southwest side of the disk is tilted toward Earth while the disk rotates in a clockwise direction in a Keplerian velocity pattern (figs. S4 to S7) (*17*). It is most likely that the observed NW and SE spirals point away from the direction of rotation—that these are trailing spiral arms.

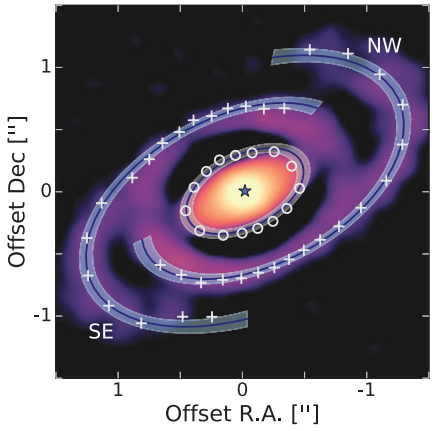

Fig. 3. Model of symmetric spirals and dark ring for the Elias 2-27 protoplanetary disk. The local maxima (crosses) and local minima (circles) in the continuum emission of Elias 2-27 are indicated. The maxima trace the NW and SE spirals, and the minima trace a ring. A model with symmetric spirals that shares the same geometry (inclination and position angle) with the inner dark ring was able to reproduce the location of the local maxima and minima of emission, as illustrated by the best-fit model (solid curve) and 3σ constraints (shaded regions). The blue star denotes the position of Elias 2-27. To illustrate the location of these features in the image, we overlaid these results over the unsharp masked image from Fig. 1B; however, this image was not used for the calculations.

Simulations indicate that planet–companion-disk interactions (PDIs) alone are capable of opening a gap creating density and temperature contrasts along spiral arms that are consistent with the observed values in NW and SE (*1*, *6*). However, the observed gap at 70 AU is of low contrast, which is indicative of a narrow or partially opened gap as predicted from PDIs with low-mass planets. Such planets will have a harder time exciting spiral density waves of the observed contrast in Elias 2-27 (*27*). Grain growth could in principle create such a low-contrast gap at 70 AU, but we see no evidence of this process in our 9 mm observations from the Karl G. Jansky Very Large Array (fig. S8) (*17*). Additionally, PDI simulations generally predict spiral arms with different contrasts to each other, unlike the similar contrast of NW and SE. Those models often struggle to produce the symmetric spiral pattern observed in the Elias 2-27 disk (*27*, *28*), unless the planet-induced density waves are driven by a massive companion at large disk radii exterior to the spirals (*6*), of which we see no evidence in the Elias 2-27 system.

Alternatively, gravitational instabilities (GIs) can also excite spiral density waves with contrasts in density and temperature that are similar to the observed contrasts in NW and SE. A high mass accretion rate, on the order of 10^{-6} to $10^{-7}\,M_{\odot}$ year^{-1} (*29*), coupled with a large disk-to-star mass ratio of at least $M_{\rm disk}/M_{\rm star} \approx 0.5$ (*3*) are required to induce the "grand design" symmetric spiral arms observed in Elias 2-27. Although the mass accretion rate of the star is high (*25*), even in the most optimistic case the disk-to-star mass ratio is $M_{\rm disk}/M_{\rm star} \approx 0.3$, limiting the possibility of GI acting alone. Additionally, simulations of disks undergoing GI generally cannot maintain spiral arms at radii larger than 100 AU because the disk begins to fragment at large radii (*2*, *3*, *29*–*31*). A possibility to avoid fragmentation in the GI scenario is that the Elias 2-27 disk is in a marginally unstable state (*32*)—for example, supported by external irradiation or sustained by an envelope that is feeding mass to the outer disk. However, no evidence for a massive envelope is found in the infrared SED of this object (*20*, *21*), making the possibility of a marginally unstable disk unlikely.

A combination of PDI and GI mechanisms acting together (*5*) could be another alternative to explain the high degree of symmetry of the arms in both contrast and location, the presence of both arms out to large disk radii, together with the gap in the disk located at 70 AU. However, this scenario also requires a high-mass planet (*5*), whose effect in the disk structure should be discernable as a larger and deeper gap than the one constrained in this work.

The observed structure in Fig. 1 delineates two symmetric trailing spiral arms, NW and SE, whose low optical depth enables material to be traced in the disk midplane. Together with the measured contrast values of at least 1.3 to 2.5 in the spiral arms, these results imply that NW and SE are tracing density and/or temperature enhancements at the disk midplane, which are arranged into two "grand design" symmetric spiral arms. Given the disk differential rotation (similar to the case of spiral galaxies), if the observed spirals were material arms rotating at the disk Keplerian velocity, then the inner part of the spiral (at 100 AU) would rotate five times faster than the outer part of the arm (at 300 AU). Thus, in a time scale much shorter than the lifetime of the disk (only a few orbital periods of roughly 1000 years) these spiral arms would wind up and disappear. We conclude that instead of tracing material arms, the NW and SE spiral structures trace density and temperature enhancements owing to spiral density waves in the midplane of the Elias 2-27 disk.

Unlike the spiral features from scattered-light observations, the spiral arms detected with our millimeter-wave imaging trace structures at the midplane of the disk—where planet formation takes place—allowing us to discern the location, shape, contrast, and size of these spiral density waves at the disk midplane. These results provide a distinct benchmark for numerical simulations of spiral structure in protoplanetary disks, particularly because fragmentation of such spirals remains the only plausible formation mechanism for planets and companions at large disk radii, where core-accretion becomes inefficient (*33*). Thus, the detection of spiral features in Elias 2-27 is a first step to determine what is the dominant mechanism of planet formation at different locations in the disk.

REFERENCES AND NOTES

1. Z. Zhu, R. Dong, J. M. Stone, R. R. Rafikov, *Astrophys. J.* **813**, 88 (2015).
2. K. M. Kratter, G. Lodato, http://arxiv.org/abs/1603.01280 (2016).
3. R. Dong, C. Hall, K. Rice, E. Chiang, *Astrophys. J.* **812**, L32 (2015).
4. M. Flock *et al.*, *Astron. Astrophys.* **574**, A68 (2015).
5. A. Pohl *et al.*, *Mon. Not. R. Astron. Soc.* **453**, 1768–1778 (2015).
6. R. Dong, Z. Zhu, R. R. Rafikov, J. M. Stone, *Astrophys. J.* **809**, L5 (2015).
7. G. Dipierro, G. Lodato, L. Testi, I. de Gregorio Monsalvo, *Mon. Not. R. Astron. Soc.* **444**, 1919–1929 (2014).
8. M. Fukagawa *et al.*, *Astrophys. J.* **636**, L153–L156 (2006).
9. J. Hashimoto *et al.*, *Astrophys. J.* **729**, L17 (2011).
10. S. P. Quanz *et al.*, *Astrophys. J.* **738**, 23 (2011).
11. T. Muto *et al.*, *Astrophys. J.* **748**, L22 (2012).
12. C. A. Grady *et al.*, *Astrophys. J.* **762**, 48 (2013).
13. M. Benisty *et al.*, *Astron. Astrophys.* **578**, L6 (2015).
14. V. Christiaens, S. Casassus, S. Perez, G. van der Plas, F. Ménard, *Astrophys. J.* **785**, L12 (2014).
15. Y. W. Tang *et al.*, *Astron. Astrophys.* **547**, A84 (2012).
16. A. Juhász *et al.*, *Mon. Not. R. Astron. Soc.* **451**, 1147–1157 (2015).
17. Materials and methods are available as supplementary materials on *Science* Online.
18. The star is also known as GSS 39, VSSG 28, GY116, and/or BKLT J162645.242309.
19. E. E. Mamajek, *Astron. Nachr.* **329**, 10–14 (2008).
20. S. M. Andrews, D. J. Wilner, A. M. Hughes, C. Qi, C. P. Dullemond, *Astrophys. J.* **700**, 1502–1523 (2009).
21. N. J. Evans II *et al.*, *Astrophys. J. Suppl. Ser.* **181**, 321–350 (2009).
22. A. Natta, L. Testi, S. Randich, *Astron. Astrophys.* **452**, 245–252 (2006).
23. A. Isella, J. M. Carpenter, A. I. Sargent, *Astrophys. J.* **701**, 260–282 (2009).
24. L. Ricci, L. Testi, A. Natta, K. J. Brooks, *Astron. Astrophys.* **521**, A66 (2010).
25. J. R. Najita, S. M. Andrews, J. Muzerolle, *Mon. Not. R. Astron. Soc.* **450**, 3559–3567 (2015).
26. C. P. Dullemond, RADMC-3D: A multi-purpose radiative transfer tool. *Astrophysics Source Code Library*, record ascl:1202.015 (2012).
27. J. Fung, R. Dong, *Astrophys. J.* **815**, L21 (2015).
28. J. Bae, Z. Zhu, L. Hartmann, *Astrophys. J.* **819**, 134 (2016).
29. C. Hall *et al.*, *Mon. Not. R. Astron. Soc.* **458**, 306–318 (2016).
30. C. J. Clarke, *Mon. Not. R. Astron. Soc.* **396**, 1066–1074 (2009).
31. P. Cossins, G. Lodato, L. Testi, *Mon. Not. R. Astron. Soc.* **407**, 181–188 (2010).
32. G. Bertin, G. Lodato, *Astron. Astrophys.* **350**, 694–704 (1999).
33. K. Rice, *Publ. Astron. Soc. Aust.* **33**, e012 (2016).

ACKNOWLEDGMENTS

We thank L. Loinard for useful discussions. L.M.P. acknowledges support from the Alexander von Humboldt Foundation. A.I. acknowledges support from NSF award AST-1109334/1535809 and from the NASA Origins of Solar Systems program through award NNX14AD26G. A.I.S. is partially supported by NSF grant AST 1140063. The National Radio Astronomy Observatory (NRAO) is a facility of the National Science Foundation (NSF) operated under cooperative agreement by Associated Universities Inc. (AUI). This paper makes use of the following ALMA data: ADS/JAO.ALMA#2013.1.00498.S, which can be obtained from the ALMA Science Data Archive, https://almascience.nrao.edu/alma-data (raw format) and from https://safe.nrao.edu/evla/disks/elias2-27 in the calibrated fits format used for analysis here. ALMA is a partnership of the European Southern Observatory (ESO) (representing its member states), NSF (USA) and the National Institute of Natural Sciences (Japan), together with the National Research Council (Canada), National Science Council and Academia Sinica's Institute of Astronomy and Astrophysics (Taiwan), and the Korea Astronomy and Space Science Institute (Republic of Korea), in cooperation with the Republic of Chile. The Joint ALMA Observatory is operated by ESO, AUI/NRAO, and the National Astronomical Observatory of Japan. Part of this research was carried out at the Jet Propulsion Laboratory, California Institute of Technology, under a contract with NASA.

SUPPLEMENTARY MATERIALS

www.sciencemag.org/content/353/6307/1519/suppl/DC1
Materials and Methods
Figs. S1 to S8
References (*34*–*49*)

6 April 2016; accepted 5 September 2016
10.1126/science.aaf8296

Spiral density waves in a young protoplanetary disk

Laura M. Pérez, John M. Carpenter, Sean M. Andrews, Luca Ricci, Andrea Isella, Hendrik Linz, Anneila I. Sargent, David J. Wilner, Thomas Henning, Adam T. Deller, Claire J. Chandler, Cornelis P. Dullemond, Joseph Lazio, Karl M. Menten, Stuartt A. Corder, Shaye Storm, Leonardo Testi, Marco Tazzari, Woojin Kwon, Nuria Calvet, Jane S. Greaves, Robert J. Harris and Lee G. Mundy

Science **353** (6307), 1519-1521.
DOI: 10.1126/science.aaf8296